

**Supporting Information for the manuscript titled:
Effect of Reversible Dislocation-Based Deformation on Nanoparticle Strain at Failure**

Claire Zhang¹, Amit Kumar Prasad², Ting Liu¹, Tevis D.B. Jacobs², Ashlie Martini¹

¹) Department of Mechanical Engineering, University of California, Merced, Merced, CA 95340, USA

²) Department of Mechanical Engineering and Materials Science, University of Pittsburgh, Pittsburgh, PA 15261, USA

Section S1: Additional information about the simulations

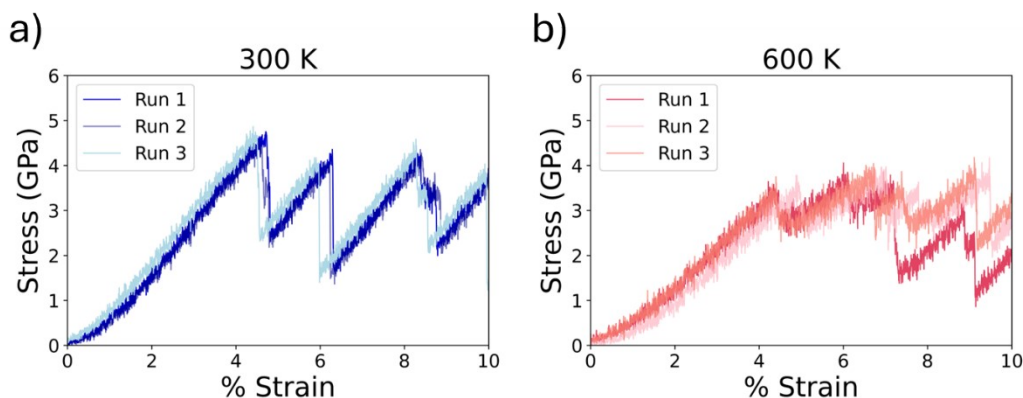


Figure S1: Stress-strain curves from three independent simulations exhibit similar magnitudes and trends. The stress-strain curves at (a) 300 K and (b) 600 K experience stress drops at similar levels of strain and are not significantly different from each other. Particles were equilibrated at each respective temperature with three distinct particle configurations taken from different times during the equilibration process then used for the compression simulation.

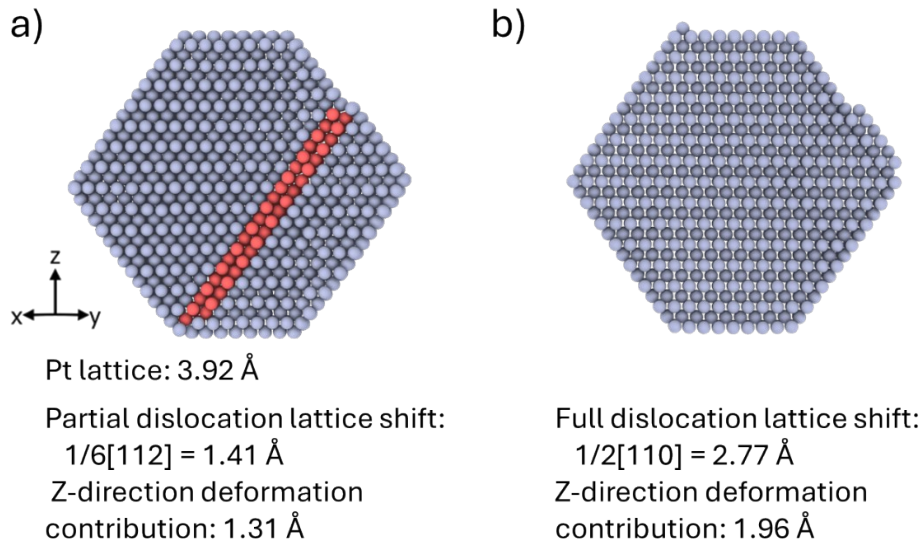


Figure S2: Irreversible deformation calculated from the lattice shift caused by particle spanning dislocations is consistent with that calculated by the freeze-release method. The expected lattice shifts of a (a) partial dislocation (lattice is not preserved) and (b) full dislocation (lattice is preserved) in the z-direction were calculated according to their Burgers vectors and the Pt lattice constant. The associated Burgers vector of a partial dislocation is $1/6 \langle 1 \ 1 \ 2 \rangle$. The length of this Burgers vector in Pt (lattice constant of 3.92 Å) is 1.41 Å. The vertical component of this Burgers vector in the z-direction was then calculated to be 1.31 Å. This is comparable to the deformation calculated using the freeze-release method of 1.26 Å. The associated Burgers vector of a full dislocation is $1/2 \langle 1 \ 1 \ 0 \rangle$. The length of this Burgers vector is 2.77 Å. The vertical component of this Burgers vector in the z-direction was then calculated to be 1.96 Å, comparable to the deformation calculated using the freeze-release method of 2.08 Å.

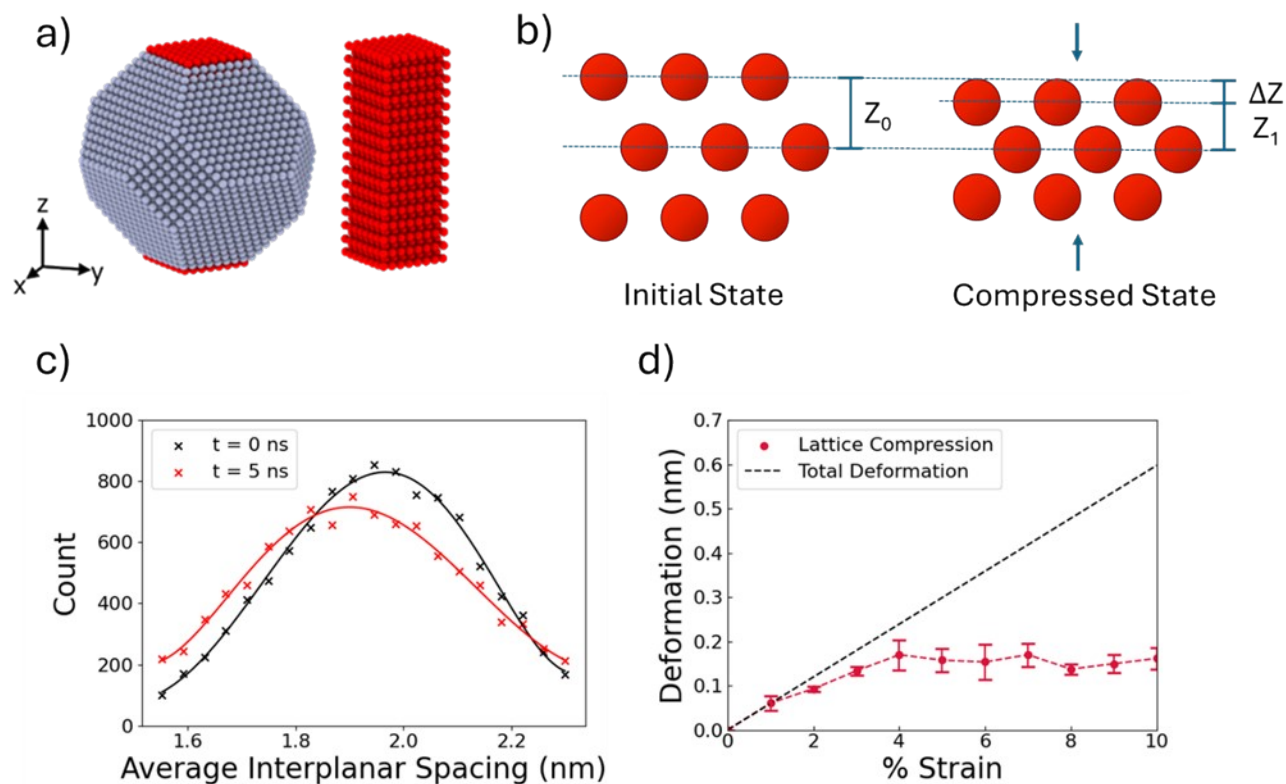


Figure S3: Lattice Compression contribution to deformation is calculated from interplanar spacing. (a) The center column of atoms between the facets in contact with the virtual walls considered for calculating lattice compression. The interplanar spacing of the initial state of nanoparticle was compared to that of the compressed state as represented by the schematic in (b), where Z_0 is the interplanar spacing of the initial state, Z_1 is the interplanar spacing of the compressed state, and ΔZ is the difference between Z_0 and Z_1 . (c) Example of a calculation of the interplanar spacing at 0 ns (initial) and 5 ns (representative compressed state) by constructing a 1D histogram of the z-direction distance between nearest neighbor atoms, fitting to a polynomial curve, and taking the maximum as interplanar distance. The difference between initial state interplanar spacing and interplanar spacing at 1% strain intervals was then multiplied by number of layers of atoms in the nanoparticle in the z direction to find (d) the total deformation due to lattice compression as a function of strain. At lower temperatures, the initial interplanar spacing was adjusted to the true lattice parameter as the equilibration process resulted in a small degree of reduced interplanar spacing even before compression.

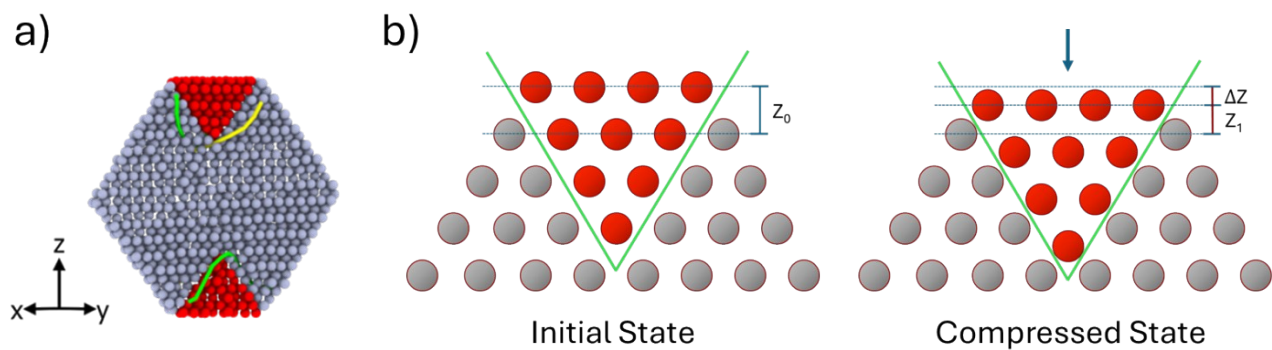


Figure S4: The contribution of entangled dislocations to deformation is calculated from the displacement of atoms enclosed by the pyramidal slip plane configuration. (a) A representative snapshot of the pyramidal area of atoms (highlighted in red) enclosed by entangled dislocations. To find the displacement of the enclosed atoms, the positions of adjacent atoms on either side of the slip plane boundary (highlighted in green) of the initial state of nanoparticle was compared to that of the compressed state as represented by the schematic in (b), where Z_0 is the initial z-direction interatomic distance, Z_1 interatomic distance of the compressed state, and ΔZ is the difference between Z_0 and Z_1 . This difference is the entangled dislocation contribution to deformation.

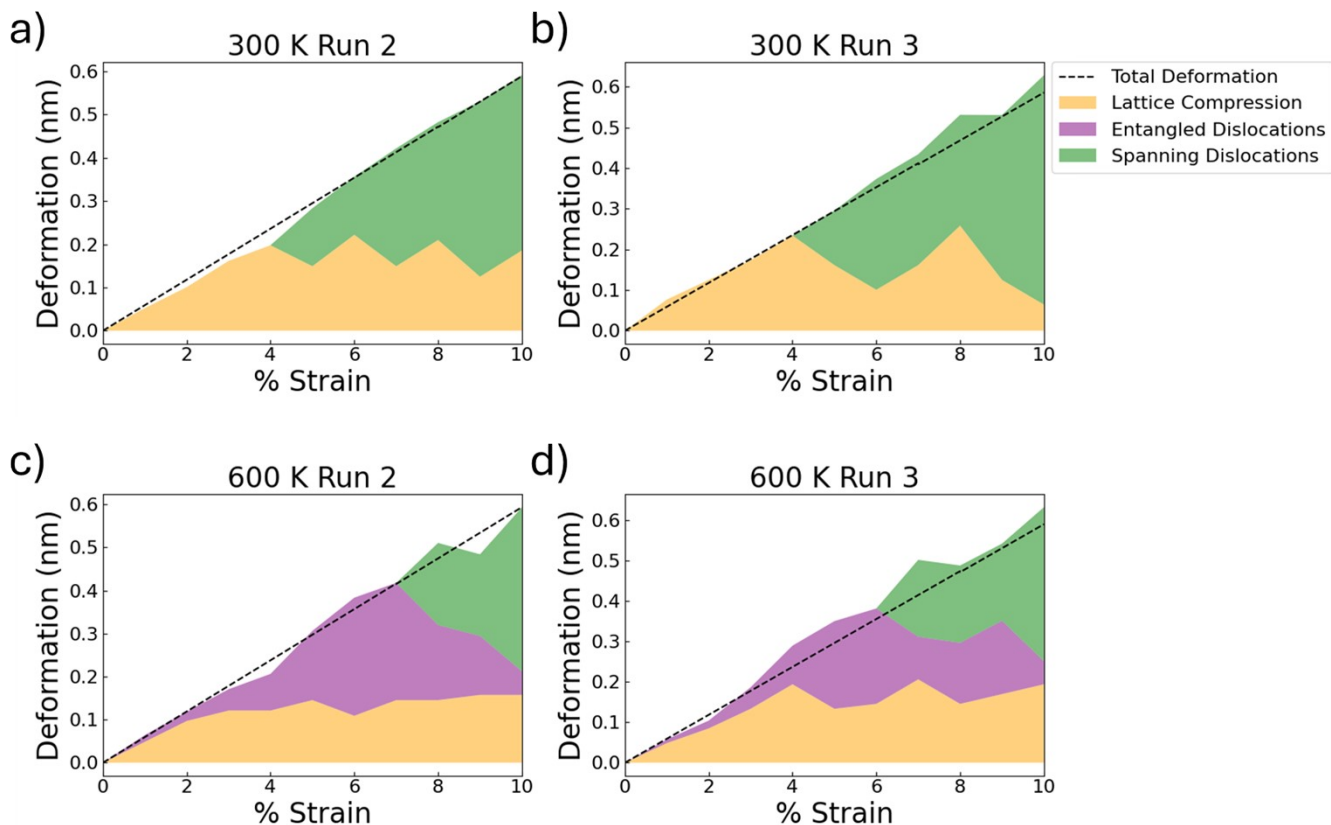


Figure S5: Additional stacked plots of the contribution of individual deformation mechanisms. Representative stacked plots of the contribution of individual deformation mechanism at (a,b) 300 K and (c,d) 600 K. The dashed line represents the imposed deformation on the nanoparticle, while yellow represents lattice compression, purple represents entangled dislocations, and green represents spanning dislocations. At 300 K, there was no contribution from entangled dislocations whereas, at 600 K, a significant contribution from entangled dislocations was observed.

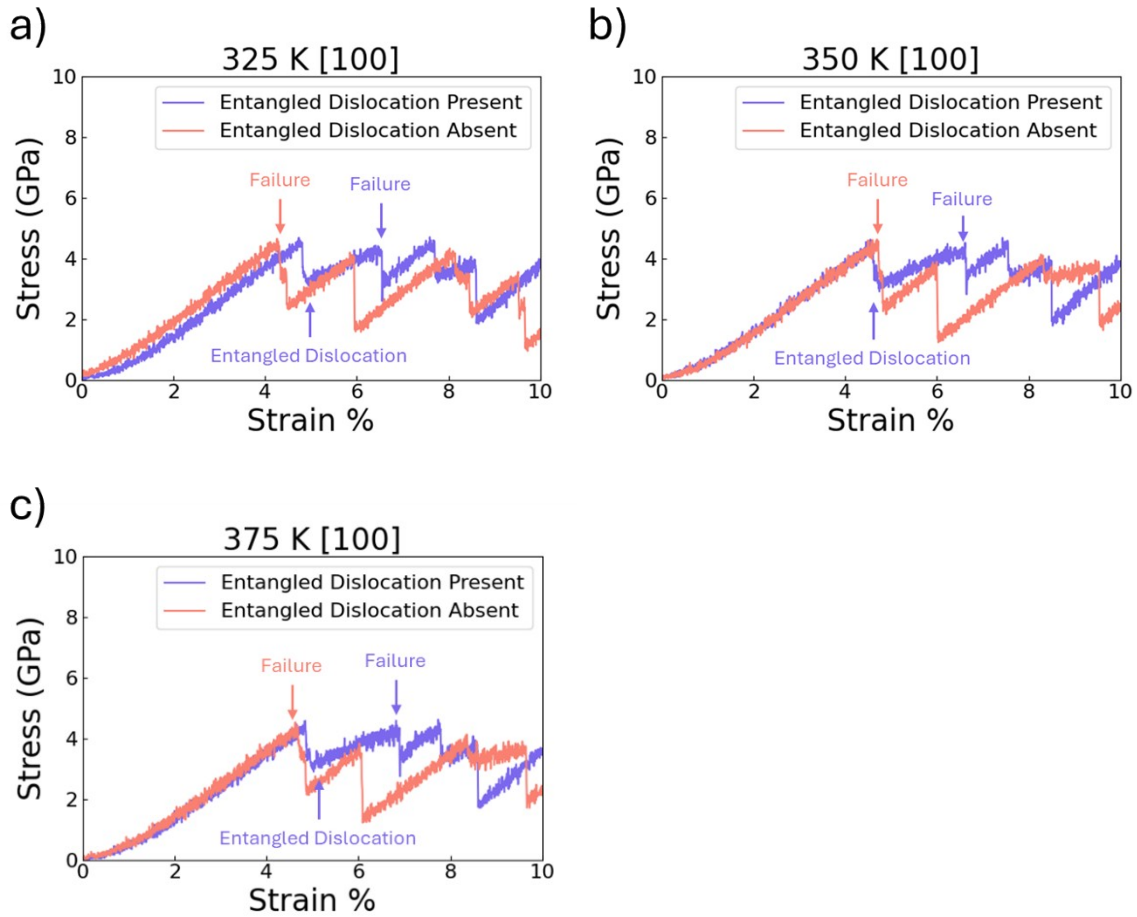


Figure S6: Dislocations between 300 and 400 K are observed at similar stress levels but can either be spanning dislocations or entangled dislocations. Representative stress-strain curves from simulations (a) 325 K, (b) 350 K, and (c) 375 K showing one case each of entangled dislocations being absent or present for temperature. Orange and violet color schemes are used for cases where entangled dislocations are absent and present, respectively. Dislocation propagation was exhibited at similar stress levels for each temperature but could have been either a spanning or entangled dislocation. When the dislocation was a spanning dislocation, the nanoparticle underwent irreversible deformation and exhibited failure. When the dislocation was an entangled dislocation, stress dropped as the entangled dislocation was able to accommodate an amount of strain, and dislocation motion was locked. Additional strain was required to build up stress back to the threshold necessary for dislocation propagation. Once stress hit this threshold, dislocation propagation resumed and the entangled dislocation evolved into a spanning dislocation, undergoing irreversible deformation and exhibiting failure.

Section S2: Methods for in situ TEM compression experiments

Simulations were complemented by real-time in situ compression testing of platinum nanoparticles. Wedge-shaped silicon substrates (Bruker, Billerica, MA) underwent plasma cleaning followed by a 20 nm cerium oxide layer deposition using sputtering (Nexdep, Angstrom Engineering, Kitchener, Canada). The choice of cerium oxide, with its superior thermodynamic stability compared to silicon oxide, was a significant factor in the process. Subsequently, 5 nm of platinum was deposited on the substrate's surface via electron-beam evaporation (MEB 550-S, Plassys, Marolles-en-Hurepoix, France). The samples were then annealed in an air atmosphere furnace (Thermolyne 1200 °C $7 \times 5 \times 10$ in., ThermoFisher Scientific, Waltham, MA) at 720 °C causing the continuous thin layer to dewet and form nanoparticles of the desired size range (80-100 nm).

In situ compression testing was carried out within a transmission electron microscope (Titan Themis G2 200, Thermo Fisher Scientific, Waltham, MA) operating at an accelerating voltage of 200 kV. An in situ nanomanipulator (Biasing Manipulator Model 1800, Hummingbird Scientific, Lacey, WA) was used with a commercial AFM probe (Tap300DLC, BudgetSensors, Sofia, Bulgaria) as an indenter and load sensor. The AFM probes, which had a nominal stiffness constant of 40 N/m, were individually calibrated using a version of Sader's method using an atomic force microscope (Tap300DLC, BudgetSensors, Sofia, Bulgaria).⁴⁸ Nanoparticles were deposited on a wedge-shaped substrate, using the method described previously in Kosinova et al. and Bechelany et al.^{49,50} The calibrated AFM probe and the nanoparticle-containing substrate were mounted on the fixed and movable side of the holder, respectively. Loading was controlled using the piezoactuator, with a loading/unloading rate of 10 nm/s. The real-time in situ experiments were recorded using a charge-coupled-device camera at an exposure time of 0.25 s/frame. Video post-processing was performed with ImageJ, and the strain of nanoparticles was analyzed from individual video frames (as described in Ding et al.).¹⁵ The instantaneous applied force was determined from an instantaneous measurement of the deflection of the calibrated AFM probe.

Supplementary Video S1: This video is a real-time recording of an in situ TEM compression that showed clear evidence of dislocations, as indicated in the still frames in Fig X of the main text. The upper portion of the video (lighter-colored shape that is roughly triangular) shows the indenter, which is composed of the sharp tip of a silicon AFM probe, that is mounted to a cantilever (off screen) that serves as a load sensor. The lower portion of the video (darker-colored shapes) shows the movable substrate (which is roughly planar) and a single platinum nanoparticle (with an initial shape similar to an irregular hexagon) that is in contact with the indenter. As the test progresses, the substrate is moved upwards, increasing the applied force on the nanoparticle. As the video progresses, the shape of the nanoparticle evolves, and deformation mechanisms appear and disappear as loading progresses. Eventually the substrate is moved back downward, such that the indenter is separated from the nanoparticle. A low frame rate was used for the video capture, in order to sacrifice time resolution in favor of spatial resolution and image clarity. The originally gray-scale video has been artificially colored to facilitate visualization of dislocations.